Inorganic Chemistry

Article

pubs.acs.org/IC

Photophysics and Nonlinear Absorption of Gold(I) and Platinum(II) Donor−Acceptor−Donor Chromophores

Subhadip Goswami, Russell W. Winkel, and Kirk S. Schanze*

Department of Chemistry, Center for Macromolecular Science and Engineering, University of Florida, P.O. Box 117200, Gainesville, Florida 32611, United States

Supporting Information

ABSTRACT: A series of Au(I) and Pt(II) acetylide complexes of a π-conjugated donor−acceptor−donor (D-A-D) chromophore were studied to develop quantitative structure−property relationships for their photophysical and nonlinear optical properties. The D-A-D chromophore consists of a "TBT" unit, where T = 3-hexyl-2,5-thienylene and BTD = 2,1,3-benzothiadiazole, capped with ethynylene groups. The D-A-D chromophore is functionalized with Au(I)PR_3 (R = −Me and −Ph) and *trans*-Pt(II)$(PR_3)_2$-CCPh (R = −Me and −Bu) "auxochromes". All of the metal complexes were characterized by ground-state absorption, photoluminescence, nanosecond transient absorption, and two-photon absorption (2PA) spectroscopy. The experiments provided quantitative values of the photophysical parameters, including rates for radiative decay and intersystem crossing (ISC), triplet yields, and two-photon absorption cross sections. Pronounced solvatochromism in the fluorescence spectra suggests an enhanced dipole moment in the excited state of the complexes compared to the unmetalated TBT chromophore. The gold complexes feature larger fluorescence quantum yields and longer emission lifetimes compared to platinum. The Pt(II) complexes exhibit enhanced triplet−triplet absorption, reduced triplet-state lifetimes, and larger singlet oxygen quantum yields, consistent with more efficient ISC compared to the Au(I) complexes. When excited by 100 fs pulses, all of the D-A-D chromophores exhibit moderate two-photon absorption in the near-infrared between 700 and 900 nm. The 2PA cross section for the Au(I) complexes is almost the same as the unmetalated D-A-D chromophore (∼100 GM). The Pt(II) complexes exhibit significantly enhanced 2PA compared to the other chromophores, reaching 1000 GM at 750 nm. Taken together, the results indicate that the Pt(II) center is considerably more effective in inducing singlet−triplet ISC and in enhancing the 2PA cross section. This result reveals the greater promise for Pt(II) acetylides in chromophores for temporal and frequency agile nonlinear absorption.

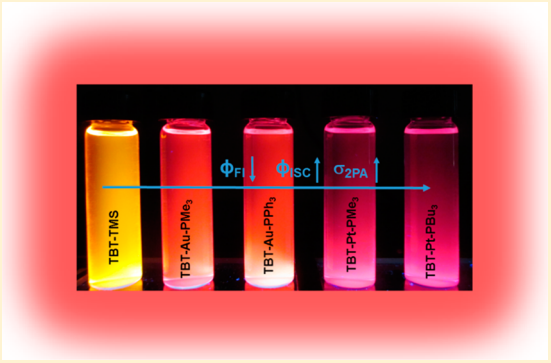

INTRODUCTION

Organometallic π-conjugated materials have emerged as a frontier research field over the past few decades, owing to their application in organic light emitting diodes,[1−3] organic photovoltaic devices,[4−7] and as materials for nonlinear absorption.[8−10] Two-photon absorption (2PA) is an important mechanism for nonlinear absorption. After 2PA was first theoretically predicted in the 1930s[11] and after its first experimental observation in 1961,[12] there has been growing interest in the development of new materials that exhibit a large 2PA cross section. Two-photon absorption has applications including optical power limiting,[13−15] imaging, data storage,[16] and photodynamic therapy.[17] Among various organometallic chromophores, heavy atom-containing π-conjugated molecules are unique in achieving efficient nonlinear absorption by a "dual mode" pathway because of the facility of harvesting triplet excited states via the spin−orbit coupling effect.[8,18] The dual mode pathway involves a combination of the $S_0 \rightarrow S_1$ transition via absorption of 2PA or 1PA followed by intersystem crossing (ISC) to the triplet excited state and excited-state absorption from $T_1 \rightarrow T_n$.[18]

The general design strategy for efficient 2PA chromophores involves molecules with a large transition dipole moment as well as permanent dipole moment between ground state (g) and excited state (e).[19] This is achieved by using donor (D) and acceptor (A) chromophores with a π-conjugated spacer in several motifs that includes D-π-A, D-π-D and A-π-A.[19] Apart from that, the D-A-D structural motif is popular for generating quadrupolar chromophores for applications not only in nonlinear absorption but also in optoelectronic devices such as organic solar cells.[4,20]

Among different organometallic architectures, metal−acetylide-containing small molecules and polymers are of interest due to strong interactions between the metal d-orbitals and the π-system of the ligand mediated via the metal−acetylide linkage.[21] In the present investigation, we explored the

Received: August 5, 2015
Published: October 6, 2015

DOI: 10.1021/acs.inorgchem.5b01767
Inorg. Chem. 2015, 54, 10007−10014

properties of ET-BTD-TE (E = ethynylene, T = 3-hexyl-2,5-thienylene, BTD = 2,1,3-benzothiadiazole) containing organometallic complexes for optoelectronic properties as well as 2PA, where BTD acts as an acceptor and T acts as a donor (Chart 1).

Chart 1

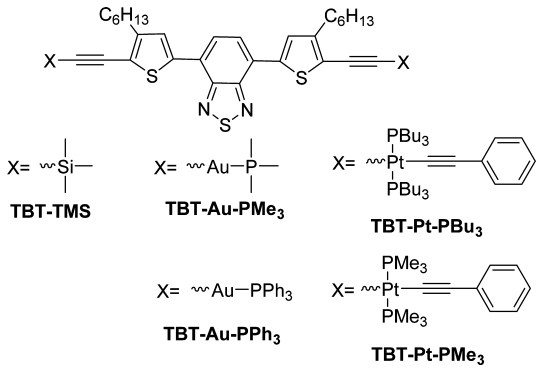

While this paper was under preparation Angelis and co-workers reported platinum and ruthenium acetylide complexes of the same ligand studied here as efficient second-order nonlinear optical chromophores.[22]

In previous work we reported a comparative study of gold(I) and platinum(II) acetylide systems with a thienyl carbazole chromophore.[23] It was observed from the low-temperature photoluminescence study that gold(I) is less efficient in promoting ISC compared to platinum(II). Because of low fluorescence quantum yield of those metal complexes and polymer, the nonlinear transmission (NLT) method was employed to characterize their 2PA behavior. However, in this previous study no clear evidence was observed for a difference between Au(I) or Pt(II) in the 2PA spectra.

To address this issue, the current work comprises the synthesis of four different gold(I) and platinum(II) complexes of the ET-BTD-TE ligand with complete photophysical characterization, including ground-state absorption, emission, nanosecond transient absorption, and singlet oxygen sensitization yields. The relatively high fluorescence quantum yields of the metal complexes allows 2PA measurement via two photon excited fluorescence method (2PEF). To understand the effect of the phosphine ancillary ligands on the photophysical properties, two gold(I) complexes were synthesized with trimethyl phosphine and triphenyl phosphine ligands (**TBT-Au-PMe$_3$** and **TBT-Au-PPh$_3$**, respectively), and two platinum(II) complexes were synthesized with trimethyl phosphine and tributyl phosphine ligands (**TBT-Pt-PMe$_3$** and **TBT-Pt-PBu$_3$**, respectively). The results clearly suggest that the platinum complexes have significantly higher triplet yields, enhanced polarizability, and 2PA cross sections compared to the gold complexes, and they have potential to be used as efficient optical power-limiting chromophores.

EXPERIMENTAL SECTION

Synthesis. The synthetic scheme, details of the synthetic procedures, along with the characterization details, are provided in the Supporting Information.

Instrumentation and Methods. All the NMR spectra were recorded by using an INOVA 500 FT-NMR operating at 500 MHz for ^{1}H NMR, operating at 125 MHz for ^{13}C NMR, or a Mercury-300 FT-NMR operating at 75.4 MHz for ^{13}C NMR and 121 MHz for ^{31}P NMR. The mass spectral analyses for the newly synthesized complexes were recorded by the Mass Spectrometry Services at University of Florida.

Photophysical measurements were performed with dry and HPLC-grade tetrahydrofuran (THF) in a 1 × 1 cm^2 quartz cuvettes unless otherwise noted. All the solutions for photophysical characterizations were prepared by diluting a stock solution unless otherwise mentioned. Ground-state UV−visible absorption spectra were obtained on a Shimadzu UV-1800 dual beam spectrophotometer. Corrected room-temperature emission spectra were obtained on a Photon Technology International (PTI) spectrophotometer and collected at 90° relative to the excitation beam. The optical density of the solutions for fluorescence quantum yield and molar extinction coefficient were kept less than or equal to 0.1. Refractive index corrections for solvents were employed for fluorescence quantum yield calculations for both sample and standard solutions. Fluorescence lifetimes were recorded with a PicoQuant FluoTime 100 Compact Fluorescence Lifetime Spectrophotometer using time-correlated single photon counting (TCSPC) instrument. The sample solutions were excited with a PDL-800B Picosecond Pulsed Laser (375 nm), and the absorbance of the solution was kept at ∼0.1.

Nanosecond transient absorption spectroscopy was performed on a home-built instrument using the third harmonic of a Continuum Surelite series Nd:YAG laser (λ_{exc}= 355 nm, 10 ns fwhm, 7 mJ per pulse). Probe light for this pump−probe spectroscopy was produced by a xenon flash lamp, and the signal was detected with a gated-intensified CCD mounted on a 0.18 M spectrograph (Princeton PiMax/Acton Pro 180). The concentrations of the sample solutions were adjusted to give O.D. ≈ 0.7 at 355 nm wavelength and were deoxygenated with argon for 45 min to 1 h before the measurement. The solutions were taken in 1 cm path length flow cell (10 mL) and continuously circulated at the pump−probe region during the experiment.

The cyclic voltammetry (CV) study of the samples was obtained on a BAS CV-50W voltammetric analyzer (Bioanalytical Systems, Inc., www.bioanalytical.com) in dry and freshly distilled dichloromethane (CH_2Cl_2) solution in the presence of 0.1 M tetra-*n*-butylammonium hexafluorophosphate ($TBAPF_6$) as electrolyte. Three electrodes were used during the measurement, namely, a platinum microdisk (2 mm^2) as the working electrode, a platinum wire as the auxiliary electrode and a silver wire as the reference electrode. The sample concentration was adjusted to 1 mM, and the sweep rate was maintained at 100 mV/s. A positive pressure of argon was maintained during the measurement. All the electrochemical potentials obtained were calibrated with respect to a ferrocene internal standard ($E(Fc/Fc^+)$ = 0.43 V vs saturated calomel electrode in CH_2Cl_2).

For 2PA absorption experiments, a Spectra-Physics Millenia eV laser (second harmonic of Nd:YAG, 532 nm) was used to pump a mode-locked Spectra-Physics Tsunami femtosecond Ti:sapphire laser. The Tsunami provides an 80 MHz pulse train of 100 fs pulses that can be tuned from 700−1000 nm. One- and two-photon excited fluorescence spectra were collected on a SPEX Fluoromax spectrophotometer. Two-photon absorption spectra and cross sections (σ_2) experiments were performed using the two-photon excited fluorescence method (2PEF), with rhodamine 6G as the reference compound and using the literature-reported values for (σ_2) and 2PA spectra.[24,25] All of the 2PA measurements were performed with air-saturated solutions.

All calculations were performed using density functional theory (DFT) as implemented in Gaussian 09 Revision C.01.[26] Geometries were optimized using the B3LYP functional along with the 6-31G(d) basis set for C, H, N, the 6-31+G(d) basis set for P, S, and the SDD basis set for Au, Pt. To minimize computational cost, solubilizing butyl moieties were replaced with methyl groups, and thiophene hexyl groups were replaced by hydrogen. Thus, only one Pt complex was computed, as they only differed in length of the solubilizing alkyl chains. These models are designated by the addition of a prime (′) to their name; thus, the model for **TBT-Pt-PMe$_3$** is termed as **PtMe′**. All singlet optimizations were initiated from idealized geometries without symmetry constraints. Triplet optimizations were initiated from the optimized singlet geometry and used the unrestricted B3LYP

DOI: 10.1021/acs.inorgchem.5b01767
Inorg. Chem. 2015, 54, 10007−10014

functional. All optimized structures were characterized by vibrational frequency calculations and were shown to be minima by the absence of imaginary frequencies. Time-dependent DFT calculations were performed for all optimized structures at the same level of theory with the same basis sets. Structures and orbitals were visualized using Chemcraft Version 1.7,[27] which was also used to generate charge-difference density plots.

RESULTS AND DISCUSSION

Electrochemistry. In an attempt to identify the effect of the heavy metals on the redox properties of the TBT moiety, CV was performed in dry dichloromethane solvent. In this experiment platinum was used as working and counter electrodes, and Ag/Ag^+ was used as quasi-reference electrode in 0.1 M NBu_4PF_6 electrolyte solution. All potentials were reported with respect to Fc/Fc^+ redox couple, and the potential values are listed in Table 1. Cyclic voltammograms are in Figure S16.

Table 1. Electrochemical Properties of the Platinum Complexes[a]

	$E_{1/2}$, V		$E_{1/2}$, V			
compound	red_1	red_2	ox_1	ox_2	ΔE_g^{Echem}, eV[b]	ΔE_g^{opt}, eV[c]
TBT-Pt-PMe$_3$	−1.73		0.29	0.46	2.02	1.93
TBT-Pt-PBu$_3$	−1.79		0.21	0.40	2.00	1.91

[a]Measured in CH_2Cl_2 using 0.1 M NBu_4PF_6 as supporting electrolyte. It was scanned at 100 mV s^{-1}. All the potentials are referenced to Fc/Fc^+ couple as an internal standard. [b]Electrochemical band gap was calculated by taking the difference between first oxidation potential and reduction potential. [c]Optical band gap was calculated from the crossing point of the normalized absorption and emission spectra.

In general for the platinum(II) complexes, the CVs exhibit a single reversible reduction wave and two reversible oxidation waves. This feature is similar to the CV of the thiophene−benzothiadiazole−thiophene unit (without any hexyl chains on thiophene) only, which suggests that all the redox behavior is centered on the chromophore and that the metals have little influence.[4] The oxidation and reduction potentials are slightly shifted from values for previously reported platinum acetylide complexes with similar TBT π-conjugated chromophore, but lacking the hexyl chain at the 3-position of the thiophenes.[4] There is a small difference in redox potentials between **TBT-Pt-PMe$_3$** and **TBT-Pt-PBu$_3$**. The first oxidation potential for **TBT-Pt-PBu$_3$** (0.21 V) is slightly less positive compared to that for **TBT-Pt-PMe$_3$** (0.29 V), and this is probably due to increased electron density in the former by tributylphosphine group. For the same reason, the reduction potential for **TBT-Pt-PBu$_3$** (−1.79 V) is more negative compared to **TBT-Pt-PMe$_3$** (−1.73 V). Unfortunately, the gold(I) complexes exhibited irreversible waves in the CV experiments, which is in accordance with the literature report from Castellano and co-workers on gold(I)-containing phenanthroline complexes.[28] The behavior is likely due to loss of the Au(I) centers concomitant with oxidation or reduction of the complexes. The electrochemical band gap for the platinum complexes was calculated by taking the difference between first oxidation and reduction potential values. Tributylphosphine substituted **TBT-Pt-PBu$_3$** has slightly smaller bandgap compared to **TBT-Pt-PMe$_3$**, which is in agreement with the optical band gap calculated from crossing point of the normalized absorption and emission spectra.

UV−visible Absorption Spectroscopy. Ground-state absorption spectra of the metal complexes and unmetalated **TBT-TMS** in THF solution are presented in Figure 1A. In general the absorption spectra exhibit two bands, which is typical for BTD-containing donor−acceptor chromophores.[4,29] The high-energy band is due to the $\pi-\pi^*$ transition of the conjugated chromophore, and the low-energy transition is assigned to the charge transfer (CT) transition.[4] DFT calculations indicate that the highest occupied molecular orbital (HOMO) is delocalized across the chromophore, whereas the lowest unoccupied molecular orbital is concentrated on the BTD acceptor unit (Supporting Information), consistent with a low-energy CT band assignment. The molar extinction coefficients (ε) and absorption band maxima (λ_{max}) for the chromophores are provided in Table 2.

Inspection of the spectra shows that the absorption of the metal complexes is significantly red-shifted from the unmetalated **TBT-TMS**, suggesting an increase in conjugation through mixing of the metal d-orbitals with the π-system of the ligand.[30] This fact is also supported by the DFT calculations where delocalization of the electron density in the HOMO is observed mediated by the metal d-orbitals (Supporting Information—computational study—Figures S20, S22, and S24). However, there are significant differences across the series. The onset of absorption for the gold complexes **TBT-Au-PMe$_3$** and **TBT-Au-PPh$_3$** is blue-shifted compared to the platinum complexes of the series **TBT-Pt-PMe$_3$** and **TBT-Pt-PBu$_3$**. The enhanced

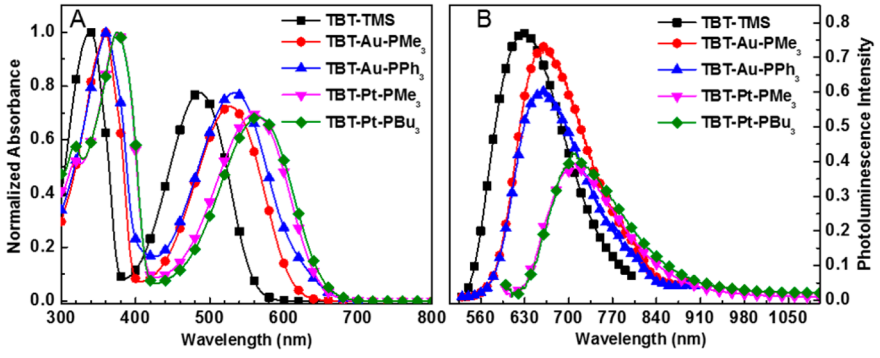

Figure 1. (A) Ground-state absorption spectra of the metal complexes and **TBT-TMS** in THF solution. (B) Photoluminescence spectra of the metal complexes and **TBT-TMS** in THF solution. The emission spectra were obtained by exciting the sample solutions at 570 nm for the metal complexes and at 500 nm for unmetalated **TBT-TMS**. Emission spectra are normalized to reflect the relative emission quantum yields of the different chromophores.

DOI: 10.1021/acs.inorgchem.5b01767
Inorg. Chem. 2015, 54, 10007−10014

Table 2. Summary of Photophysical Properties[a]

compound	λ_{max} (nm)	ε (M^{-1} cm^{-1})	λ_{em} (nm)	Φ_{fl}[b]	k_r (1×10^8 s^{-1})	k_{isc} (1×10^7 s^{-1})	Φ_{isc}	τ_{fl} (ns)	τ_{TA} (μs)	Φ_{Δ}[c] (%)
TBT-TMS	487	33 000	628	0.77	1.0			7.5		
TBT-Au-PMe$_3$	519	27 000	659	0.73	1.1	1.1	0.10	6.5	2.14	9
TBT-Au-PPh$_3$	527	30 000	654	0.60	1.0	3.3	0.20	6.3	1.54	17
TBT-Pt-PMe$_3$	555	35 000	696	0.39	1.0	11	0.46	4.4	1.43	31
TBT-Pt-PBu$_3$	566	32 000	704	0.42	1.0	11	0.45	4.3	1.10	26

[a]All the photophysical properties were recorded in THF; λ_{max} is the absorption maxima, ε is the molar extinction coefficient, λ_{em} is the emission band maxima, Φ_{fl} is the fluorescence quantum yield, k_r, k_{isc}, and Φ_{isc} are the rate constant for radiative decay, rate constant for ISC, and the ISC quantum yield, respectively, τ_{fl} and τ_{TA} are the lifetime of fluorescence and triplet excited state, respectively, Φ_{Δ} is the singlet oxygen quantum yield. [b]Fluorescence quantum yield was measured with respect to Rhodamine B as actinometer in absolute ethanol (Φ_{fl} = 0.49). [c]Singlet oxygen quantum yield was measured in C_6D_6 using terthiophene (Φ_{Δ} = 0.73) as actinometer.

conjugation for platinum acetylides can be attributed to better orbital overlap of Pt-5d orbitals with the π-orbitals of the TBT chromophore,[31] and also the DFT calculation provides evidence for contribution of additional terminal acetylide group of the platinum acetylides to the HOMO (Figures S20 and S24). Interestingly for both gold(I) and platinum(II) complexes there are differences observed in the absorption spectra at longer wavelength with change in ancillary phosphine ligand. Specifically, there is an ∼8 nm red shift in λ_{max} of absorption for **TBT-Au-PPh$_3$** in comparison to **TBT-Au-PMe$_3$**. However, λ_{max} of absorption for **TBT-Pt-PBu$_3$** is ∼11 nm red-shifted compared to **TBT-Pt-PMe$_3$**. The difference in electron-donating ability of the phosphine ligands slightly alters the charge density in metal-dπ orbitals, and hence the extent of pπ−dπ interaction also changes. This fact is indirect evidence of the contribution of metal-to-ligand charge transfer (MLCT) character to the long wavelength CT transition.

To understand the polarity of the ground state, solvent-dependent absorption spectra were measured for ligand **TBT-TMS** and metal complexes **TBT-Au-PMe$_3$** and **TBT-Pt-PMe$_3$**. The absorption spectra blue-shift with increased polarity of the solvent (Figure S17). In general the low-energy absorption band was more affected by the change in solvent polarity compared to the high-energy absorption band, likely due to its CT character. The shifts in the absorption spectra for the metal complexes are larger compared to **TBT-TMS**, possibly due to enhanced polarity of the metal complexes in ground state. The gold(I) and platinum(II) metal complexes have almost the same change in absorption spectra with solvent polarity, suggesting a similar change in dipole moment on excitation.

Steady-State Photoluminescence Spectroscopy. The photoluminescence spectra of the ligand and metal complexes were recorded in THF and shown in Figure 1B. They all exhibit a featureless broad emission band with a small Stokes shift relative to the lowest-energy absorption band. This fact along with the emission lifetimes, which are on the order of a few nanoseconds, suggest that emission can be assigned to fluorescence from the lowest singlet excited state. The trend in the emission spectra observed across the series is the same as in absorption spectra. In particular, bathochromic shifts were observed upon metalation of the ligand **TBT-TMS**, suggesting enhanced π-conjugation. As expected, the onset of emission is further red-shifted for the platinum acetylide complexes compared to the gold complexes due to the contribution of both Pt-5d orbitals and terminal acetylide moiety.

The fluorescence band maxima (λ_{em}), fluorescence quantum yields (Φ_{fl}), and lifetimes (τ_{fl}) for **TBT-TMS** and the metal complexes are listed in Table 2. All metal complexes exhibit lower Φ_{fl} and τ_{fl} compared to the unmetalated **TBT-TMS** chromophore. In general Φ_{fl} and τ_{fl} values are larger for the gold complexes than the platinum complexes. The radiative decay rates (k_r) for the metal complexes and **TBT-TMS** are calculated from the fluorescence quantum yields and lifetimes. In general, k_r remains almost the same across the series (∼1×10^8 s^{-1}). However, the difference in fluorescence quantum yields and lifetimes of the metal complexes compared to **TBT-TMS** suggests a nonradiative decay pathway is active to a varying extent. We suggest that this is due to $S_1 \rightarrow T_1$ ISC. If it is assumed the nonradiative decay rate from $S_1 \rightarrow S_0$ remains the same for the metal complexes and **TBT-TMS** ($k_{nr} \approx 3 \times 10^7$ s^{-1}), then it is possible to estimate the rate of intersystem crossing (k_{isc}) and quantum yield of intersystem crossing efficiency (Φ_{isc}) for the series. Within this approximation, it is seen that the gold complexes have k_{isc} values on the order of ∼1×10^6 s^{-1}, whereas the platinum complexes undergo ISC 3−4 times faster with a rate on the order of ($k_{isc} \approx 1 \times 10^7$ s^{-1}). Overall the platinum complexes have significantly higher Φ_{isc} values compared to the gold complexes indicating ISC is less efficient in gold(I) congeners compared to platinum(II) congeners, which is in accordance with the previous literature reports.[23,32]

The fluorescence band maxima for all of the metal complexes and **TBT-TMS** exhibit a bathochromic shift as the solvent polarity increases (Figure S17). Compared to the ground-state absorption spectra, a larger change is observed in the emission band in response to the change in solvent polarity, which is in accordance with the literature for BTD-containing donor−acceptor chromophores.[33] This is possibly due to direct excitation of the ground-state chromophores to less polar Franck−Condon excited state and then relaxation to a more polar CT excited state from where the emission occurs.[34] The excited-state dipole moments (μ_e) of the given chromophores were estimated by using Lippert−Mataga eq 1a.

$$\nu_a - \nu_f = [2(\mu_e - \mu_g)^2 \Delta f]/(hca^3) + C \quad (1a)$$

where

$$\Delta f \cong \left[\frac{\varepsilon - 1}{2\epsilon + 1} + \frac{n^2 - 1}{2n^2 + 1}\right] \quad (1b)$$

The Stokes shift ($\nu_a - \nu_f = \bar{\nu}$) is plotted as a function of the solvent polarizability (Δf) for different solvents. To calculate the excited-state dipole moment value (μ_e) from the Lippert−Mataga equation, it is necessary to estimate the ground-state dipole moment (μ_g) and the effective radii of the Onsager cavity (a). The ground-state dipole moments (μ_g) of the ligand and the metal complexes were estimated from DFT calculations performed in the gas phase (0.18 D for **TBT-TMS**, 9.62 D for

DOI: 10.1021/acs.inorgchem.5b01767
Inorg. Chem. 2015, 54, 10007−10014

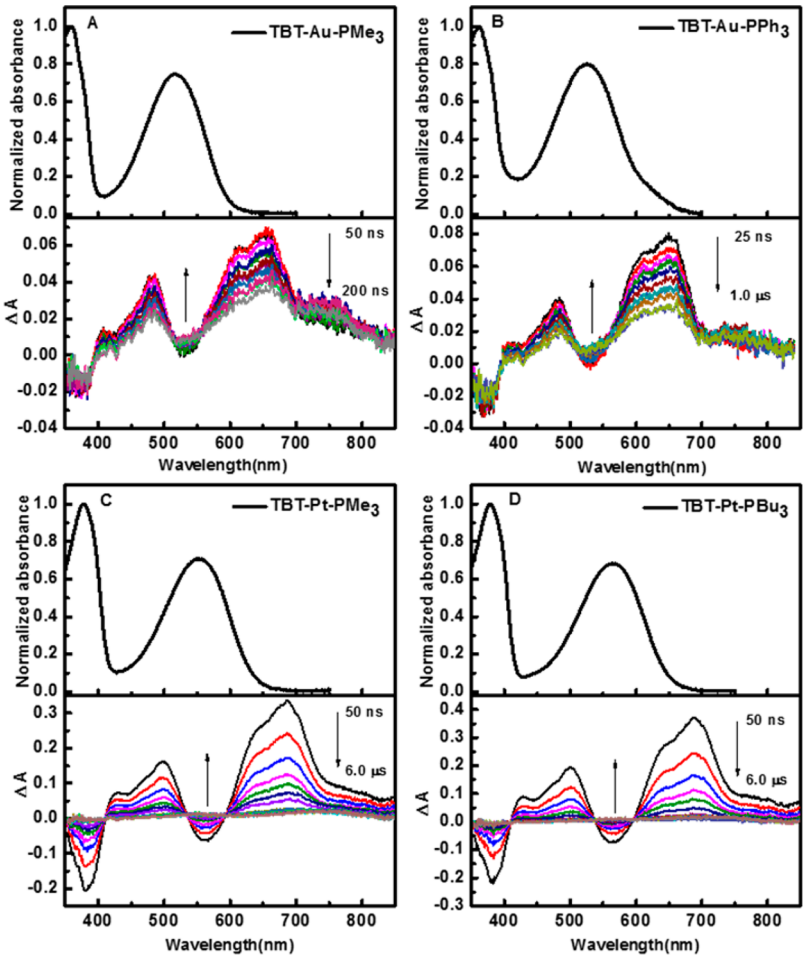

Figure 2. Ground-state absorption (upper panels) and transient absorption spectra (lower panels) of the metal complexes. Transient absorption spectra obtained in deoxygenated THF solution with λ_{exc} of 355 nm. Initial delay was 50 ns for (A, C, D) and 25 ns for (B). Delay increment was 10 ns for (A), 50 ns for (B), and 300 ns for (C, D).

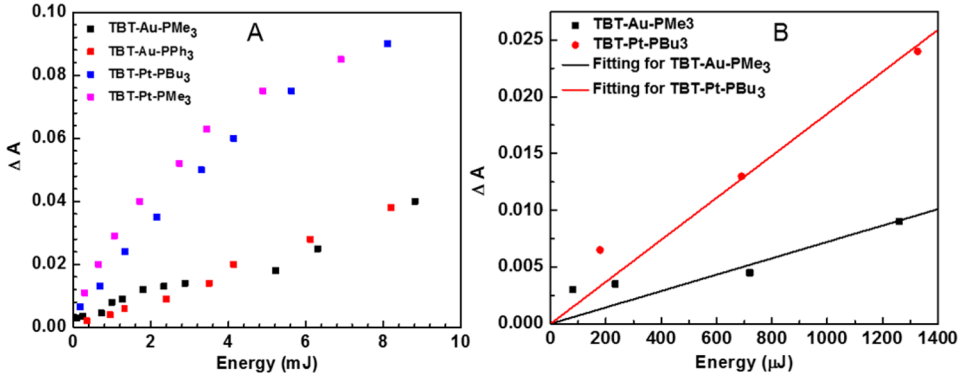

Figure 3. (A) Laser energy dependent transient absorption study of the metal complexes monitored at 480 nm. The experiment was performed with matched ground-state absorption ≈ 0.7 for all the metal complexes at 355 nm. (B) Comparison of energy dependence for **TBT-Au-PMe$_3$** and **TBT-Pt-PBu$_3$** at low laser power (0−1.4 mJ); lines represent least-squares fits of the data.

TBT-Au-PMe$_3$, and 18.6 D for **TBT-Pt-PMe$_3$**). The effective radii of Onsager cavity (a) for the metal complexes were estimated by calculating molecular dimensions from DFT (6.2 Å for **TBT-TMS**, 6.6 Å for **TBT-Au-PMe$_3$**, and 7.4 Å for **TBT-Pt-PMe$_3$**). From the slope of the linear plot along with the estimated value of Onsager cavity (a), the difference in dipole moments between ground and excited state is estimated (Figure S18). In general the positive values of $(\mu_e - \mu_g)$ suggest the increased dipole moments in the excited state. Compared to the ground state both the metal complexes and **TBT-TMS** chromophore have higher dipole moment values in excited state (11.2 D for **TBT-TMS**, 23.6 D for **TBT-Au-PMe$_3$**, and 34.6 D for **TBT-Pt-PMe$_3$**). The trend in polarity of the molecules (**TBT-TMS** < **TBT-Au-PMe$_3$** < **TBT-Pt-PMe$_3$**) remains same both in the ground and excited states.

Nanosecond Transient Absorption Spectroscopy. Since phosphorescence was not observed from the metal complexes, nanosecond transient absorption spectroscopy was

DOI: 10.1021/acs.inorgchem.5b01767
Inorg. Chem. 2015, 54, 10007−10014

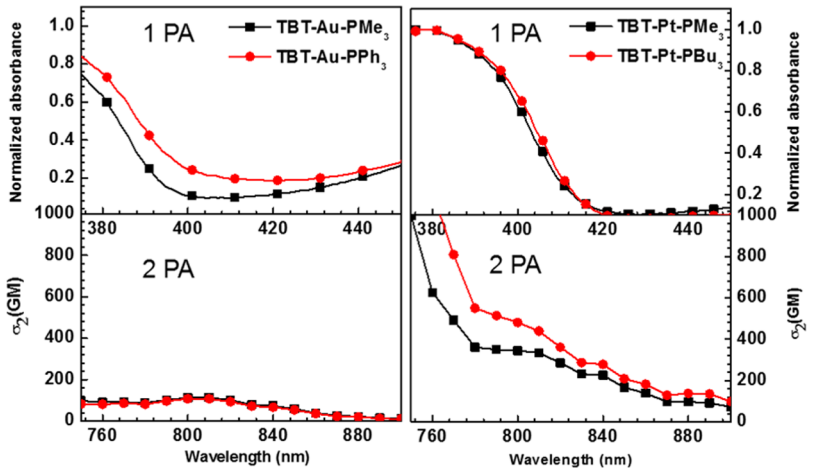

Figure 4. Two-photon absorption spectra (lower panel) and one-photon absorption spectra (upper panel) of the metal complexes in THF solution. Corresponding wavelengths are on *x*-axis. Two-photon absorption cross section and normalized absorbance are shown in the corresponding *y*-axis.

performed in deoxygenated THF to seek evidence of triplet excited-state population. Figure 2 shows the transient absorption of the metal complexes (lower panel) along with their ground-state absorption spectra (upper panel). In general all of the transient absorption spectra consist of a broad absorption band at 600−800 nm region with strong bleaching at the ground-state absorption band. All of the transients are quenched by molecular oxygen, supporting their assignment to the triplet excited state. There was no evidence of triplet−triplet absorption observed for the unmetalated chromophore **TBT-TMS**, consistent with a low ISC yield (e.g., <0.05). Careful inspection of the spectra in Figure 2 reveals that the intensity of the transient absorption for the gold(I) complexes is 4−5 times less compared to the platinum(II) complexes. As the experiment is performed with sample solutions of matched absorbance and with the same laser pulse energy, this result suggests gold(I) complexes have a lower triplet yield compared to the platinum(II) complexes.

A quantitative energy-dependent transient absorption study of the metal complexes was performed by monitoring the difference absorption at 480 nm (Figure 3A,B). Since the ground-state absorption (O.D. ≈ 0.7) at the excitation wavelength (355 nm) was the same for the samples, it is possible to estimate the relative ISC yields from the slope of ΔA versus energy plot at low excitation energy.[35] Figure 3B compares the plots for the complexes **TBT-Au-PMe$_3$** and **TBT-Pt-PBu$_3$** at low laser power. It is evident from the ratio of the slopes that the ISC efficiency for the platinum complex **TBT-Pt-PBu$_3$** is at least 2.6 times greater compared to the gold complex **TBT-Au-PMe$_3$**. A similar result is obtained for the other two metal complexes, namely, **TBT-Pt-PMe$_3$** and **TBT-Au-PPh$_3$**.

To measure the triplet excited lifetime of the metal complexes single wavelength transient absorption decays were measured, and the decay kinetics was monitored at 480 nm (Figure S25). It was found that the gold(I) complexes have slightly longer triplet-state lifetimes compared to the platinum-(II) complexes. This pattern was observed in a previous study, and it is attributed to the fact that there is less spin−orbit coupling in the gold(I) complexes, and this effect results in longer triplet lifetimes, since the triplet decay rate depends on the extent of mixing of the triplet excited state with the singlet ground state.

Singlet oxygen sensitization gives an indirect measure of the triplet yield by monitoring the phosphorescence from singlet oxygen at 1270 nm. All of the metal complexes sensitized the formation of singlet oxygen in deuterated benzene solution, and the singlet oxygen quantum yield (Φ_Δ) varies in the series **TBT-Pt-PMe$_3$** > **TBT-Pt-PBu$_3$** > **TBT-Au-PPh$_3$** > **TBT-Au-PMe$_3$** (Table 2). Note that the Φ_{ISC} values estimated from the radiative and nonradiative decay rates of the metal complexes, as described above, are in reasonable agreement with the Φ_Δ values. The platinum(II) congeners having more efficient ISC, in general, give rise to higher singlet oxygen quantum yields compared to the gold(I) complexes. Relatively higher singlet oxygen quantum yield for **TBT-Au-PPh$_3$** compared to **TBT-Au-PMe$_3$** can be attributed to efficient ISC to the triplet excited state in the former.

Two-Photon Absorption Spectroscopy. To assess 2PA spectra and cross sections (σ_2), THF solutions of these metal complexes and ligand were excited by the Ti−sapphire pumped oscillator system (pulse duration < 100 fs, 80 MHz repetition), and the results are presented in Figure 4. Because of the limitations of the laser system used, these experiments were performed over the 700−900 nm region. (It is important to note that this spectral region is 2PA degenerate with the second absorption band in the one photon spectra.) Normalized one-photon absorption spectra are shown in the same plot for comparison. In general there is a significant blue shift of 2PA spectra compared to the ground-state absorption, consistent with the centrosymmetric nature of the molecules.[36,37]

The unmetalated **TBT-TMS** chromophore has a 2PA cross section $\sigma_{2PA} \approx 120$ GM in the region between the degenerate CT and π,π^* one-photon transitions (Figure S26). The 2PA spectra of the gold(I) metal complexes show a well-defined peak at 780−800 nm and another broad absorption band at <775 nm. The 2PA spectra for the gold complexes are slightly red-shifted compared to the 2PA spectra of **TBT-TMS**. This fact can be attributed to the slight increase in conjugation length mediated by the gold dπ orbitals, and this trend is in accordance with the ground-state absorption spectra.

Although the σ_{2PA} values for the gold(I) complexes are similar to that for **TBT-TMS** at 780−800 nm, they have slightly higher values approaching 150 GM at shorter wavelength. Surprisingly, for platinum(II) complexes the σ_{2PA} values are 200−600 GM in the 800−900 nm region and approach 1000

DOI: 10.1021/acs.inorgchem.5b01767
Inorg. Chem. 2015, 54, 10007−10014

GM at $\lambda < 800$ nm. One of the main factors that influence 2PA is transition dipole moment for the ground to first excited-state transition (μ_{ge}). The dipole moment for the metal complexes in excited state is calculated from solvent-dependent emission spectra by utilizing Lippert−Mataga equation. The enhanced 2PA for the platinum(II) complexes can be explained as arising due to their larger change in dipole moment upon excitation compared to gold(I) complexes.

General Discussion. In general, heavy-atom substitution of π-conjugated chromophores enhances their nonlinear absorption arising from both instantaneous 2PA and longer time scale multiphoton absorption due to the $T_1 \rightarrow T_n$ absorption (TTA). In the present study it has been shown that 2PA and TTA are significantly enhanced by incorporation of the heavy metal centers, compared to the unmetalated chromophore. In addition, it was found that Pt(II) is much more effective than Au(I) in enhancing both nonlinear absorption mechanisms, first by enhancing σ_2 and second by increasing the triplet yield, which enhances TTA.

An important factor that contributes to the 2PA in the two-level model is the change in dipole moment between the ground and excited states, and it can be expressed by the following equation:

$$\sigma_2 = \frac{2(2\pi)^4 f_{\text{opt}}^4}{15(nch)^2} |\mu|^2 |\Delta\mu|^2 (2\cos^2\theta) g(2\upsilon_L) \quad (2)$$

where μ and $\Delta\mu$ are the transition dipole moment and the difference in permanent dipole moments between ground and excited states, respectively.[38] It can be understood from this equation that σ_2 is proportional to $\Delta\mu^2$. From the study of the solvatochromic behavior of the gold and platinum acetylide complexes it was shown that the latter exhibit larger change in dipole moment in excited state ($\Delta\mu$), and this is the reason they exhibit higher 2PA cross sections.

Davies and co-workers demonstrated that when comparing structurally analogous gold(I) and ruthenium(II) acetylide complexes, the latter feature 3−5-fold larger quadratic nonlinearity, and this effect was attributed to the electron-rich nature of ruthenium.[39] In a similar line, one possible reason for higher change in dipole moment for the platinum(II) complexes that are the subject of the present investigation is the greater π-electron donating nature of Pt(II) compared to Au(I).

In another related study, Jia and co-workers reported a family of trimetallic gold(I) and ruthenium(II) acetylide complexes with an electron-poor triazine core.[40] The ruthenium complexes were found to have significantly red-shifted absorption compared to the gold complexes. The authors showed that the HOMO of the chromophore was less influenced by gold nonbonding d-orbitals because of their comparatively low energy; however, the ruthenium dπ orbitals are situated above the HOMO energy level and significant orbital mixing provides extensive conjugation, leading to a low energy CT transition with considerable d$\pi \rightarrow \pi^*$ character. In the present study, DFT calculations on **TBT-Pt-PMe$_3$** and **TBT-Au-PMe$_3$** found that gold dπ orbitals contribute less to the HOMO in comparison to the platinum dπ orbitals, and this enhanced dπ contribution gives rise to higher polarizability in the platinum complexes (Figures S20 and S24). Unlike other transition metals, gold(I) undergoes stabilization of the filled $5d_{z^2}$ orbital by mixing with the 6s level. This high s-orbital content of the frontier orbital makes the Au(I) center isolobal with a proton.[41] This could be another reason for reduced electron delocalization in gold(I) complexes, because the interaction between the metal center and the acetylide unit is localized and dominated by σ interactions.

Finally, another striking difference observed between gold(I) and platinum(II) complexes is in their quantum yield of intersystem crossing (Φ_{ISC}). The ISC efficiency induced by a heavy atom not only depends on the spin−orbit coupling constant (which is similar for platinum and gold) but also varies significantly with orbital interaction between the heavy metal and the π-conjugated chromophore. The Pt(II) 5d orbitals interact efficiently with the π and π^* molecular orbitals of the conjugated TBT chromophore. However, for Au(I) acetylide systems, the orbital interaction between Au(I) 5d orbitals and the π-system is minimal, and it is believed that it is this factor that reduces the spin−orbit coupling and hence Φ_{ISC}.

SUMMARY AND CONCLUSIONS

In summary, a series of metal acetylide complexes with a π-conjugated D-A-D chromophore was prepared that feature Au(I) and Pt(II) "auxochromes" to study the impact on triplet excited-state properties and how 2PA is influenced by the different transition metal centers. The ground-state absorption spectra exhibit a minimal bathochromic shift for Au(I) complexes compared to Pt(II) complexes, supporting the concept of isolobal relation of Au(I) with H^+, which leads to less effective conjugation via gold center.[41] The effect of the ancillary phosphine ligands on photophysical properties and their contribution to the overall CT character of these complexes is also demonstrated. In particular, electrochemical characterization of the Pt(II) complexes suggests the more electron-rich $-PBu_3$ ligand leads to a negative shift in both the oxidation and reduction potentials of the analogous complexes with $-PMe_3$ ligands. Enhanced solvatochromic response of the metal complexes in emission spectra indicates their increased polar character in the excited state compared to the ground state. Enhanced ISC efficiency for Pt(II) is demonstrated by using fluorescence and transient absorption spectroscopy. While the gold complexes have comparable 2PA cross sections ($\sigma_2 \approx 150-200$ GM) compared to the unmetalated **TBT-TMS** chromophore, significantly higher cross sections are observed for the platinum complexes (maximum $\sigma_2 \approx 1000$ GM). DFT calculations also provide evidence for higher metal orbital contribution for Pt(II) compared to Au(I). This study provides an understanding of the importance of electron-rich, polarizable transition metals in 2PA, ISC, and the application of these chromophores for frequency and temporally agile nonlinear absorption.

ASSOCIATED CONTENT

Supporting Information

The Supporting Information is available free of charge on the ACS Publications website at DOI: 10.1021/acs.inorgchem.5b01767.

Detailed synthesis experimental procedures, including reaction schemes and experimental description, full NMR spectral characterization of all target compounds, cyclic voltammetry, and density functional calculation results, solvent-dependent absorption and emission spectra, Lippert−Mataga plot, two photon absorption spectra of the unmetalated chromophore TBT-TMS, illustrations of DFT-optimized singet (ground) state

DOI: 10.1021/acs.inorgchem.5b01767
Inorg. Chem. 2015, 54, 10007−10014

structure and molecular orbitals of AuMe′, AuPh′, and PtMe′. (PDF)

AUTHOR INFORMATION

Corresponding Author

*E-mail: kschanze@chem.ufl.edu. Phone: 352-392-9133.

Notes

The authors declare no competing financial interest.

ACKNOWLEDGMENTS

This work was supported by the National Science Foundation (Grant No. CHE-115164). The authors acknowledge the Univ. of Florida Research Computing (http://researchcomputing.ufl.edu) for providing computational resources and support that have contributed to the research results reported in this publication. The authors acknowledge Dr. R. Acharya for performing some absorption measurements needed for the revision.

REFERENCES

(1) Forrest, S. R.; O'Brien, D. F.; You, Y.; Shoustikov, A.; Sibley, S.; Thompson, M. E.; Baldo, M. A. *Nature* **1998**, *395*, 151−154.
(2) Giridhar, T.; Saravanan, C.; Cho, W.; Park, Y. G.; Lee, J. Y.; Jin, S.-H. *Chem. Commun.* **2014**, *50*, 4000−4002.
(3) Rausch, A. F.; Murphy, L.; Williams, J. A. G.; Yersin, H. *Inorg. Chem.* **2012**, *51*, 312−319.
(4) Mei, J.; Ogawa, K.; Kim, Y.-G.; Heston, N. C.; Arenas, D. J.; Nasrollahi, Z.; McCarley, T. D.; Tanner, D. B.; Reynolds, J. R.; Schanze, K. S. *ACS Appl. Mater. Interfaces* **2009**, *1*, 150−161.
(5) Baek, N. S.; Hau, S. K.; Yip, H.-L.; Acton, O.; Chen, K.-S.; Jen, A. K. Y. *Chem. Mater.* **2008**, *20*, 5734−5736.
(6) Zhen, H.; Hou, Q.; Li, K.; Ma, Z.; Fabiano, S.; Gao, F.; Zhang, F. *J. Mater. Chem. A* **2014**, *2*, 12390−12396.
(7) Bertrand, G. H. V.; Tortech, L.; Gandon, V.; Aubert, C.; Fichou, D. *Chem. Commun.* **2014**, *50*, 8663−8666.
(8) Rogers, J. E.; Slagle, J. E.; Krein, D. M.; Burke, A. R.; Hall, B. C.; Fratini, A.; McLean, D. G.; Fleitz, P. A.; Cooper, T. M.; Drobizhev, M.; Makarov, N. S.; Rebane, A.; Kim, K.-Y.; Farley, R.; Schanze, K. S. *Inorg. Chem.* **2007**, *46*, 6483−6494.
(9) Dubinina, G. G.; Price, R. S.; Abboud, K. A.; Wicks, G.; Wnuk, P.; Stepanenko, Y.; Drobizhev, M.; Rebane, A.; Schanze, K. S. *J. Am. Chem. Soc.* **2012**, *134*, 19346−19349.
(10) Yi, J.; Zhang, B.; Shao, P.; Li, Y.; Sun, W. *J. Phys. Chem. A* **2010**, *114*, 7055−7062.
(11) Göppert-Mayer, M. *Ann. Phys.* **1931**, *401*, 273−294.
(12) Kaiser, W.; Garrett, C. G. B. *Phys. Rev. Lett.* **1961**, *7*, 229−231.
(13) Hrobárik, P.; Hrobáriková, V.; Semak, V.; Kasák, P.; Rakovský, E.; Polyzos, I.; Fakis, M.; Persephonis, P. *Org. Lett.* **2014**, *16*, 6358−6361.
(14) Purc, A.; Sobczyk, K.; Sakagami, Y.; Ando, A.; Kamada, K.; Gryko, D. T. *J. Mater. Chem. C* **2015**, *3*, 742−749.
(15) Westlund, R.; Malmström, E.; Lopes, C.; Öhgren, J.; Rodgers, T.; Saito, Y.; Kawata, S.; Glimsdal, E.; Lindgren, M. *Adv. Funct. Mater.* **2008**, *18*, 1939−1948.
(16) Gao, Y.; Qu, Y.; Jiang, T.; Zhang, H.; He, N.; Li, B.; Wu, J.; Hua, J. *J. Mater. Chem. C* **2014**, *2*, 6353−6361.
(17) Schmitt, J.; Heitz, V.; Sour, A.; Bolze, F.; Ftouni, H.; Nicoud, J.-F.; Flamigni, L.; Ventura, B. *Angew. Chem., Int. Ed.* **2015**, *54*, 169−173.
(18) Liao, C.; Shelton, A. H.; Kim, K.-Y.; Schanze, K. S. *ACS Appl. Mater. Interfaces* **2011**, *3*, 3225−3238.
(19) He, G. S.; Tan, L.-S.; Zheng, Q.; Prasad, P. N. *Chem. Rev.* **2008**, *108*, 1245−1330.
(20) Ellinger, S.; Graham, K. R.; Shi, P.; Farley, R. T.; Steckler, T. T.; Brookins, R. N.; Taranekar, P.; Mei, J.; Padilha, L. A.; Ensley, T. R.; Hu, H.; Webster, S.; Hagan, D. J.; Van Stryland, E. W.; Schanze, K. S.; Reynolds, J. R. *Chem. Mater.* **2011**, *23*, 3805−3817.
(21) Grelaud, G.; Cifuentes, M. P.; Paul, F.; Humphrey, M. G. *J. Organomet. Chem.* **2014**, *751*, 181−200.
(22) Colombo, A.; Nisic, F.; Dragonetti, C.; Marinotto, D.; Oliveri, I. P.; Righetto, S.; Lobello, M. G.; De Angelis, F. *Chem. Commun.* **2014**, *50*, 7986−7989.
(23) Goswami, S.; Wicks, G.; Rebane, A.; Schanze, K. S. *Dalton Trans.* **2014**, *43*, 17721−17728.
(24) Xu, C.; Webb, W. W. *J. Opt. Soc. Am. B* **1996**, *13*, 481−491.
(25) Makarov, N. S.; Drobizhev, M.; Rebane, A. *Opt. Express* **2008**, *16*, 4029−4047.
(26) Frisch, M. J.; Trucks, G. W.; Schlegel, H. B.; Scuseria, G. E.; Robb, M. A.; Cheeseman, J. R.; Scalmani, G.; Barone, V.; Mennucci, B.; Petersson, G. A.; et al.; Gaussian Inc.: Wallingford, CT, 2009.
(27) Zhurko, G. A. http://www.chemcraftprog.com, 2012.
(28) Pomestchenko, I. E.; Polyansky, D. E.; Castellano, F. N. *Inorg. Chem.* **2005**, *44*, 3412−3421.
(29) Shang, H.; Fan, H.; Liu, Y.; Hu, W.; Li, Y.; Zhan, X. *Adv. Mater.* **2011**, *23*, 1554−1557.
(30) Frapper, G.; Kertesz, M. *Inorg. Chem.* **1993**, *32*, 732−740.
(31) Li, P.; Ahrens, B.; Bond, A. D.; Davies, J. E.; Koentjoro, O. F.; Raithby, P. R.; Teat, S. J. *Dalton Trans.* **2008**, 1635−1646.
(32) Zhou, G.-J.; Wong, W.-Y. *Chem. Soc. Rev.* **2011**, *40*, 2541−2566.
(33) Pina, J.; de Melo, J. S.; Breusov, D.; Scherf, U. *Phys. Chem. Chem. Phys.* **2013**, *15*, 15204−15213.
(34) Karunakaran, V.; Prabhu, D. D.; Das, S.; Varughese, S. *Phys. Chem. Chem. Phys.* **2015**, *17*, 18768.
(35) This assumes that the molar extinction coefficient of the triplet excited state is the same for the two complexes at the wavelength where the transient absorption is monitored. This is clearly an approximation.
(36) Terenziani, F.; Painelli, A.; Katan, C.; Charlot, M.; Blanchard-Desce, M. *J. Am. Chem. Soc.* **2006**, *128*, 15742−15755.
(37) Barzoukas, M.; Blanchard-Desce, M. *J. Chem. Phys.* **2000**, *113*, 3951−3959.
(38) Rebane, A.; Drobizhev, M.; Makarov, N. S.; Beuerman, E.; Haley, J. E.; Krein, D. M.; Burke, A. R.; Flikkema, J. L.; Cooper, T. M. *J. Phys. Chem. A* **2011**, *115*, 4255−4262.
(39) Whittall, I. R.; Humphrey, M. G.; Samoc, M.; Luther-Davies, B. *Angew. Chem., Int. Ed. Engl.* **1997**, *36*, 370−371.
(40) Hu, Q. Y.; Lu, W. X.; Tang, H. D.; Sung, H. H. Y.; Wen, T. B.; Williams, I. D.; Wong, G. K. L.; Lin, Z.; Jia, G. *Organometallics* **2005**, *24*, 3966−3973.
(41) Raubenheimer, H. G.; Schmidbaur, H. *Organometallics* **2012**, *31*, 2507−2522.

DOI: 10.1021/acs.inorgchem.5b01767
Inorg. Chem. 2015, 54, 10007−10014